Synthesis, Electrochemical Properties, and Phase Stability of Li_2NiO_2 with the *Immm* Structure

Kisuk Kang,† Ching-Hsiang Chen,‡ Bing Joe Hwang,‡ and Gerbrand Ceder*,†

Department of Materials Science and Engineering, Massachusetts Institute of Technology, 7 Massachusetts Avenue, Cambridge, Massachusetts, 02139, and Microelectrochemistry Laboratory, Department of Chemical Engineering, National Taiwan University of Science and Technology, 43 Keelung Road, Section 4, Taipei 106, Taiwan, ROC

Received January 13, 2004. Revised Manuscript Received April 26, 2004

The electrochemical properties and phase stability of the orthorhombic *Immm* structure of composition Li_2NiO_2 are studied experimentally and with first principles calculations. The material shows a high specific charge capacity of about 320 mAh/g and discharge capacity of about 240 mAh/g at the first cycle. The experimental results and first principles calculations all indicate that the orthorhombic *Immm* structure is rather prone to phase transformation to a close-packed layered structure during the electrochemical cycling. The possibility of stabilizing the orthorhombic *Immm* structure during the electrochemical cycling by partial substitution of Ni is also evaluated. A detailed analysis of the crystal field energy difference between octahedral and square-planar coordinated Ni^{2+} indicates that crystal field effects may not be large enough to stabilize Ni^{2+} in a square planar environment when the cost of electron pairing is taken into account. Rather, we attribute the stability of Li_2NiO_2 in the *Immm* structure to the more favorable Li arrangement as compared to a possible Li_2NiO_2 structure with octahedral Ni.

Introduction

There has been extensive research to develop a new positive electrode for rechargeable Li batteries with high specific capacity. Of particular attention recently has been the Ni^{2+}/Ni^{4+} redox couple, which has been shown to exchange two electrons in layered $LiNi_{0.5}Mn_{0.5}O_2$, $Li_{0.9}Ni_{0.45}Ti_{0.55}O_2$, and spinel $LiNi_{0.5}Mn_{1.5}O_4$.[1−6] Such a redox couple with multiple oxidation states opens up the potential for a significant increase in specific capacity. In these materials, Ni is cycled from +2 to +4 in a reasonable voltage range, while Mn or Ti is electrochemically inactive. Theoretically, if the electrochemically inactive Mn or Ti can be removed from the structure, and Ni is the only transition metal in the structure, the specific capacity can be almost doubled. A composition such as Li_2NiO_2 has a theoretical specific capacity of 513 mAh/g. Previously, Dahn et al. obtained 1T-Li_2NiO_2 by over-lithiation of layered $LiNiO_2$ with the $R\bar{3}m$ structure.[7] 1T-Li_2NiO_2 is isostructural with $Ni(OH)_2$ [Figure 1(a)] and forms a layered structure with layers of octahedral Ni and tetrahedral Li alternating between the close-packed oxygen planes. Hence, upon over-discharge of $R\bar{3}m$ $LiNiO_2$, all the octahedral Li ions are moved into tetrahedral sites, as 1T-Li_2NiO_2 is formed. Because of the large electrostatic repulsion between the tetrahedral Li ions in 1T-Li_2NiO_2, there is a large potential step when going from $LiNiO_2$ to 1T-Li_2NiO_2.

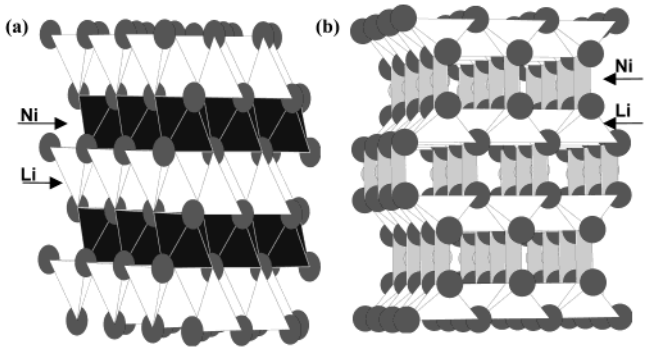

Figure 1. Crystal structure of (a) 1T-Li_2NiO_2 (Ni occupies the center of the octahedron (dark shaded) and Li occupies the center of a tetrahedron (light shaded)); (b) I-Li_2NiO_2 (Ni occupies the center of the rectangle (dark shaded) and Li occupies the center of a tetrahedron (light shaded).)

The groundstate of Li_2NiO_2 is not the 1T structure, but an orthorhombic form with *Immm* space group. Indeed, upon heating 1T-Li_2NiO_2, it converts to the *Immm* structure.[7] In this work we synthesize the *Immm* form directly and investigate its electrochemical activity. *Immm*-Li_2NiO_2 (I-Li_2NiO_2, hereafter) can be described

* Corresponding author. E-mail: gceder@mit.edu.
† Massachusetts Institute of Technology.
‡ National Taiwan University of Science and Technology.

(1) Lu, Z.; MacNeil, D. D.; Dahn, J. R. *Electrochem. Solid State Lett.* **2001**, *4*, A191.
(2) Ammundsen, B.; Paulsen, J. *Adv. Mater.* **2001**, *13*, 943.
(3) Ohzuku, T.; Makimura, Y. *Chem. Lett.* **2001**, 744.
(4) Reed, J.; Ceder, G. *Electrochem. Solid State Lett.* **2002**, *5* (7), A145.
(5) Kang, K.; Carlier, D.; Reed, J.; Arroyo, E.; Ceder, G.; Croguennec, L.; Delmas, C. *Chem. Mater.* **2003**, *15*, 4503.
(6) Zhong, Q.; Bonakdarpour, A.; Zhang, M.; Gao, Y.; Dahn, J. R. *J. Electrochem. Soc.* **1997**, *144*, 205.
(7) Dahn, J. R.; von Sacken, U.; Michal, C. A. *Solid State Ionics* **1990**, *44*, 87.

10.1021/cm049922h CCC: $27.50
Published on Web 06/05/2004

as a structure with chains of edge-shared [NiO_4] squares where Ni is at the center of the oxygen rectangle. Li occupies tetrahedral sites as seen in Figure 1b. We will discuss the electrochemical properties and structural phase stability of I-Li_2NiO_2 on the basis of experimental results and first principles calculations.

Methods

Sample Preparation. Li_2NiO_2 was prepared by solid-state reaction of NiO and Li_2O (99.5%, Alfa Aesar). NiO was obtained from calcination of Ni_2CO_3 (99%, Alfa Aesar) at 400 °C for several hours. The appropriate amounts of these starting materials were ball-milled in an Ar environment for one day. After recovering the mixture, it was pressed into a pellet. The pellet was heated at 650 °C for 24 h in a homemade Ni tube filled with Ar.

X-ray Diffraction. The XRD pattern was recorded using a Rigaku diffractometer equipped with Cu Kα radiation by step scanning (0.01°/1 s) in the 2θ range of 10−80°. The structure was refined with Fullprof.[8]

Electrochemical Testing. The lithium cells were configured in the following way. Li/$LiPF_6$ (1M) in EC/DMC (1:1; Merck)/Li_2NiO_2 with carbon black (15 wt %) used as conductive agent and polyethylenetetrafluoride (PTFE; 5 wt %) as binder. Cells were assembled in an argon-filled glovebox and cycled at room temperature using a Maccor 2200 operating in galvanostatic mode. The electrochemical performance of the sample was evaluated upon cycling in the 1.5−4.5 -V potential window at current density 0.5 mA/cm^2 (12.5 mA/g) rate.

First Principles Calculation. All energies used for the phase stability study and potential prediction are calculated with the spin-polarized generalized gradient approximation to density functional theory, using a plane-wave basis set and the projector-augmented wave method as implemented in the Vienna ab initio simulation package (VASP). A plane-wave basis with a kinetic energy cutoff of 400 eV was used, and reciprocal-space *k*-point grids between 12 × 14 × 8 and 8 × 8 × 8 were used depending on the structure and the size of the supercell considered. All structures were fully relaxed. For structures in which Ni ions carry a magnetic moment, the difference between antiferromagnetic and ferromagnetic spin ordering was considered. The difference in energy between spin configurations was never more than 50 meV per Ni, and for all cases tested, the ferromagnetic state was the ground state. Voltages were calculated as outlined in previous work.[9]

X-ray Absorption Spectroscopy Measurement. In-situ X-ray absorption spectra (XAS) have been recorded at beam line BL17C of the National Synchrotron Radiation Research Center (NSRRC) at Hsinchu, Taiwan. The storage ring was operated with an electron energy of 1.5 GeV and a current between 100 and 200 mA. Data collection was carried out in the transmission mode with a Si(111) double-crystal monochromator. High-order harmonics were eliminated by adjusting the parallelism of the monochromator crystals. The intensities of incident and transmitted beams were monitored using ionization chambers as detectors. The absorption of Ni metal foil was measured in transmission between the second and third ionization chambers to calibrate the energy scale of the monochromator simultaneously. During in situ XAS measurements, the beam size was limited by the horizontal and vertical slits with the area of 2 × 2 mm^2.

EXAFS Data Analysis. Standard procedures were followed to analyze the EXAFS data. First, the raw absorption spectrum in the preedge region was fitted to a straight line and the background above the edge was fitted with a cubic spline. The EXAFS function χ was obtained by subtracting the postedge background from the overall absorption and then normalized with respect to the edge jump step. The normalized χ(E) was transformed from energy space to *k* space, where *k* is the photoelectron wave vector. The $\chi(k)$ data described the oscillation of the backscattering wave through the local environment of about ∼10 Å. For the Li_2NiO_2 material, the k^3-weighted EXAFS spectra, $k^3 \cdot \chi(k)$, for the selected absorber Ni, were calculated to compensate the damping of the EXAFS oscillations in the high-*k* region. Subsequently, k^3-weighted $\chi(k)$ data in the *k* space ranging from 3.45 to 10.31 $Å^{-1}$ was Fourier transformed (FT) to *r* space to separate the EXAFS contributions from different coordination shells. A nonlinear least-squares algorithm was applied for curve fitting of the EXAFS results in *r* space between 0.92 and 3.04 $Å^{-1}$.

The structure parameters such as coordination numbers (*N*), bond distances (*R*), and Debye−Waller factor were extracted by curve-fitting analysis based on Winxas2.3. The theoretical EXAFS parameters, the backscattering amplitude and the phase shift, were calculated using the FEFF7 code[10] for all possible scattering paths which were generated on the basis of known structures. The amplitude reduction factor S_0^2 was scaled to a fixed value of 0.812 after preliminary refinements.

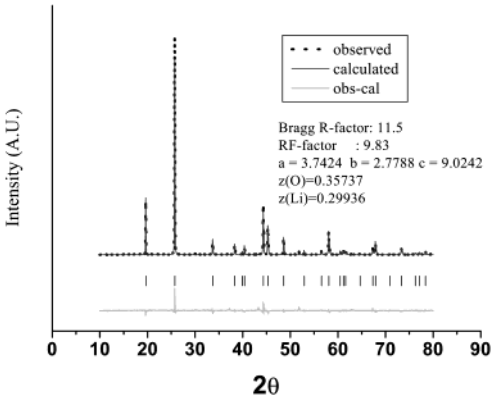

Figure 2. XRD pattern and Rietveld refinement of Li_2NiO_2 (*a*, *b*, and *c* are the lattice parameters and *z* is the atomic position of oxygen or Li along the *c* axis.)

Results

Structural Analysis of I-Li_2NiO_2. Figure 2 shows the XRD pattern and lattice parameters of Li_2NiO_2. Below the measured diffraction pattern are the calculated pattern for the orthorhombic *Immm* structure with Ni in 2a (0, 0, 0) sites, Li in 4i (0, 0, *z*(Li)) sites, and O in 4j (0.5, 0 ,*z*(O)) sites, and the difference between the calculated and observed patterns. A trace of a NiO phase is observed. The amount of NiO could be reduced, though not eliminated, by increasing the reaction time, adding extra Li to the synthesis, and reducing the particle size of the reagents. The refined structure parameters are in good agreement with previous studies.[11] The calculated lattice parameters from the first principles ($a = 3.803$, $b = 2.808$, $c = 8.936$ Å) also agree with the refined values within about 2%.

Electrochemical Properties. The charge−discharge curves of a cell with a Li_2NiO_2 cathode are shown in galvanostatic mode in Figure 3. The first charging capacity is about 320 mAh/g and the first discharge capacity is about 240 mAh/g at 12.5 mA/g rate, indicating a significant capacity loss in the first cycle. The

(8) Fullprof available at http://www-llb.cea.fr/winplotr/winplotr.htm.
(9) Aydinol, M. K.; Kohan, A. F.; Ceder, G.; Cho, K.; Joannopoulos, J. *Phys. Rev. B* **1997**, *56*, 1354.
(10) Zabinsky, S. I.; Rehr, J. J.; Ankudinov, A.; Eller, M. *J. Phys. Rev. B.* **1995**, *52*, 2995.
(11) Rieck, H.; Hoppe, R. *Z. Anorg. Allg. Chem.* **1972**, *392*, 193.

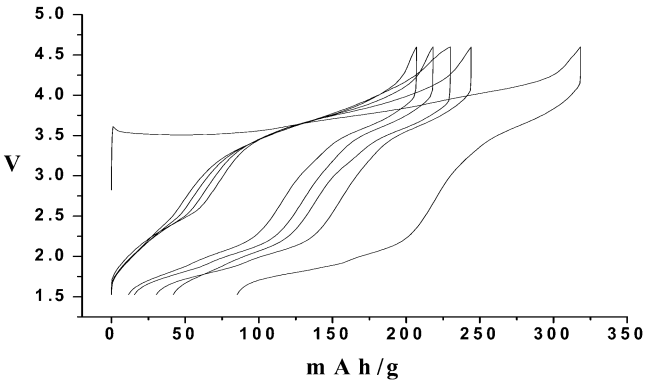

Figure 3. Charge−discharge curves for Li_2NiO_2 cycled in the voltage range 1.5−4.6 V at the current density of 12.5 mA/g.

capacity is far less than the theoretical capacity (513 mAh/g) based on the Ni^{2+}/Ni^{4+} redox couple. The first charge curve is clearly different from other charge curves and is never recovered in the consecutive charging, whereas the first discharge curve is almost identical with other discharge curves. These results seem to indicate that an irreversible structural change occurs during the first cycle. In the discharge profile, there are clearly two plateaus observed at about 3.7 V and 1.9 V, respectively. These plateaus are also present in the charge curve after the first cycle. These two plateaus occur at potentials characteristic of the layered $LiNiO_2$−layered NiO_2 reaction (about 3.9 V),[12] and 1T-Li_2NiO_2−layered $LiNiO_2$ (experimentally about 1.9 V).[7]

Ex situ XRD was performed to identify a possible change in the structure. Figure 4 shows the XRD patterns of the positive electrode before and after the electrochemical cycling. After cycling, only peaks from the NiO-impurity are visible and all diffraction lines of the *Immm* material have disappeared. The lack of any diffraction peaks, besides the unreacted NiO, indicates that upon cycling I-Li_2NiO_2 has transformed completely to a material with very small crystallite size or with a fully amorphous structure. It is noticeable that even with the pseudo-amorphous XRD pattern, the electrochemical profile of the material is reminiscent of that of crystalline layered $LiNiO_2$.

First Principles Calculations. To identify the possible phase transformation, we compare the calculated energy differences between the orthorhombic *Immm* structure and the layered $R\bar{3}m$ structure as a function of the Li content. The first principles results confirm that at Li_2NiO_2 composition *Immm* is the structure with the lowest energy. However, at composition $LiNiO_2$, the layered structure is already more stable than I-Li_2NiO_2 by about 0.2 eV per formula unit. With all the lithium removed, the orthorhombic structure is extremely unstable and is about 1.5 eV per formula unit higher than that of layered NiO_2. Given this large driving force to convert to the layered form, it is unlikely that the *Immm* structure can persist at high levels of Li deintercalation.

The measured delithiation potentials can give some insight into the transformation mechanism by comparing it to the calculated potential for possible reactions. This comparison is complicated by the fact that voltages calculated with standard DFT can be significantly underpredicted.[9] Hence, we corrected the calculated potentials by +0.7 V which is approximately the error for the $LiNiO_2/NiO_2$ average potential in the layered structure.[4] Table 1 gives the average potential for delithiation with different structural transitions. For example, it can immediately be predicted from the table that there is very little possibility to obtain I-NiO_2 during the cycling because of the exceptionally high potential it takes to obtain it from $LiNiO_2$. The average potential from I-$LiNiO_2$ to I-NiO_2 is 5.04 V. It seems more likely that layered NiO_2 is formed from either I-$LiNiO_2$ (3.7 V) or layered $LiNiO_2$ (3.9 V). We cannot conclusively decide from the observed potential which structure is present at $LiNiO_2$ composition, because the difference (0.2 V) is within the uncertainty caused by the combination of DFT error and the lack of long-range crystalline order in the experimental sample.

Table 1. Calculated Voltage for Delithiation Reactions between the Possible Structures[a]

	$LiNiO_2$	I-$LiNiO_2$	1T-Li_2NiO_2	I-Li_2NiO_2
NiO_2 (layer)	3.90	3.70		
I-NiO_2	5.24	5.04		
$LiNiO_2$ (layer)			2.41	3.18
I-$LiNiO_2$			2.60	3.37

[a] All potentials are corrected by adding 0.7 V to the value obtained from DFT/GGA.[4]

By comparing the potentials shown in Table 1 with the discharge profile in Figure 3, it seems that I-Li_2NiO_2 is not recovered after full discharge. If I-Li_2NiO_2 would form from either I-$LiNiO_2$ or layered $LiNiO_2$, the plateau at the end of discharge would appear at potentials near 3.18 or 3.37 V, not at about 2 V which is what is observed in the actual discharge profile. The observed value is closer to the calculated value for the formation of 1T-Li_2NiO_2. Hence, comparison of the calculated potentials indicates that upon the first charge I-Li_2NiO_2 goes to either I-$LiNiO_2$ or layered $LiNiO_2$ which further delithiates to a layered $Li_{2-x}NiO_2$ ($x > 1$). Upon discharge the orthorhombic structure is not reformed. To confirm this and obtain more details on the extent of the transformation, an EXAFS analysis was performed.

EXAFS Analysis. EXAFS spectra are the amplitude summation of the constructive and destructive scattering, which are influenced by the local structure surrounding the target atom. The k^3-weighted EXAFS spectra and their Fourier transform (FT) at the Ni K edge for Li_2NiO_2 as a function of state of charge are shown in Figure 5a and b, respectively. The phase and amplitude of the FT spectra are uncorrected. On the basis of the crystal structure, two effective scattering paths are considered in the simulated results. From the previous XRD study, pristine Li_2NiO_2 exhibits an *Immm* space group. The first peak at ~1.5 Å is assigned to the four oxygens in the first coordination shell around Ni. Furthermore, the second peak at ~2.5 Å is assigned to the two Ni−Ni second coordination shells. The structural parameters describing the local environment for $Li_{2-x}NiO_2$ were obtained from the EXAFS data with Winxas2.3 and the FEFF7 code. In all cases, the value of the residual factor defined by the following equation

(12) Delmas, C.; Peres, J. P.; Rougier, A.; Demourgues, A.; Weill, F.; Chadwick, A.; Broussely, M.; Perton, F.; Biensan, P.; Willmann, P. *J. Power Sources* **1997**, *68*, 120.

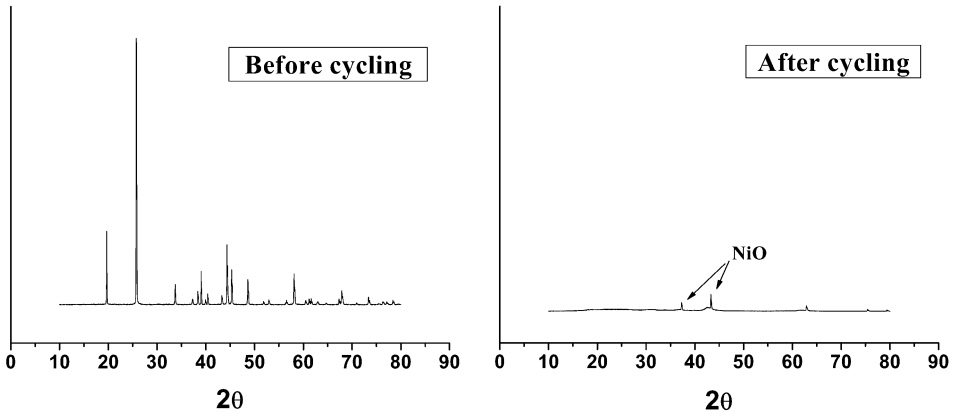

Figure 4. XRD pattern of Li_2NiO_2 before and after the cycling.

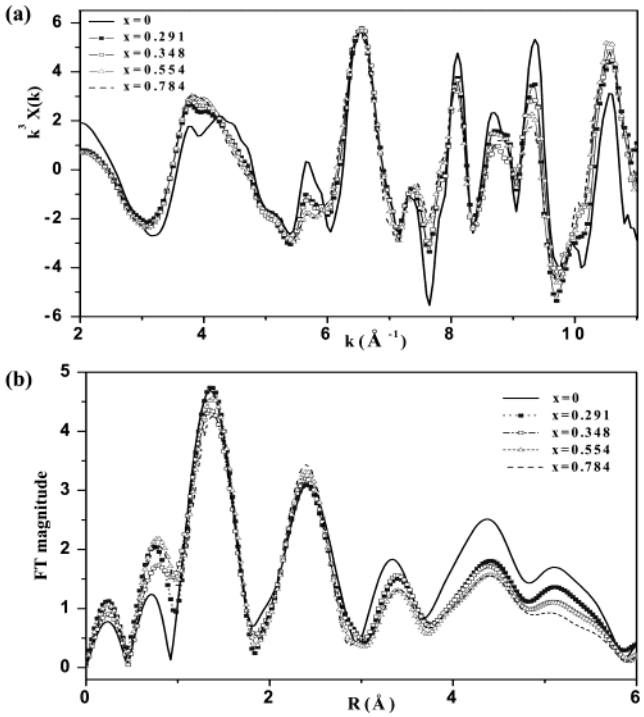

Figure 5. (a) k^3-Weighted EXAFS spectra and (b) FT magnitudes of k^3-weighted at Ni K-edge as a function of x in $Li_{2-x}NiO_2$.

is less than 10, indicating that the fitting error is quite small.

$$\text{residual factor (\%)} = \frac{\sum_{i=1}^{N}|y_{\text{exp}}(i) - y_{\text{theo}}(i)|}{\sum_{i=1}^{N}|y_{\text{exp}}(i)|} \times 100$$

where y_{exp} and y_{theo} are experimental and theoretical data points, respectively.

Figure 6 shows the change of coordination number for the Ni−O and Ni−Ni shells in Li_2NiO_2 at different charge states. The coordination numbers for the Ni−O and Ni−Ni shells are observed to increase from 3.9 to 5.4 and from 1.9 to 3.4, respectively, as deintercalation (x in $Li_{2-x}NiO_2$) increases from $x = 0$ to $x = 0.784$ during the first charging process. The ratio of the Ni−Ni coordination number to the Ni−O coordination number increases from 0.49 to 0.63.

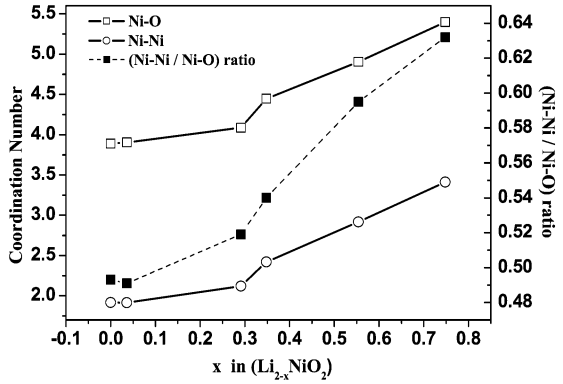

Figure 6. Coordination numbers of the Ni−O shell and Ni−Ni shell and their ratio versus x in $Li_{2-x}NiO_2$.

For a transformation from the *Immm* to the layered structure, the coordination numbers for Ni−O and Ni−Ni shells should change from 4 to 6 and 2 to 6, respectively. Meanwhile, the ratio of the Ni−Ni coordination number to the Ni−O coordination number will increase from 0.5 to 1. Considering EXAFS is an average technique, the coordination numbers probably represent a mixture of *Immm* and $R\bar{3}m$ structure. This preliminary EXAFS study implies that the *Immm* structure becomes unstable with delithiation and transforms to a layered structure during the charging process, which is consistent with the results of our first principles calculations.

Discussion

Relation of Phase Stability of I-Li_2NiO_2 to its Electronic Structure. According to the first principles calculation, I-Li_2NiO_2 has a lower energy than 1T-Li_2NiO_2. One can try to understand this in terms of the crystal field stabilization energy (CFSE) for the different Ni coordination in each structure.[13] In I-Li_2NiO_2, Ni is coordinated by four oxygens in a square planar configuration, whereas in 1T-Li_2NiO_2, Ni is octahedraly coordinated by oxygen. The electronic structure of square planar Ni^{2+} coordination can be derived from that of octahedral coordination by moving two oxygens on the z-axis of an octahedron far enough away so that Ni^{2+} effectively only interacts with the four oxygens in the $x-y$ plane. As oxygen moves away along the z-axis,

(13) Figgis, B. N.; Hitchman, M. A. *Ligand Field Theory and Its Applications*; Wiley-VCH: New York, 2000; p 112.

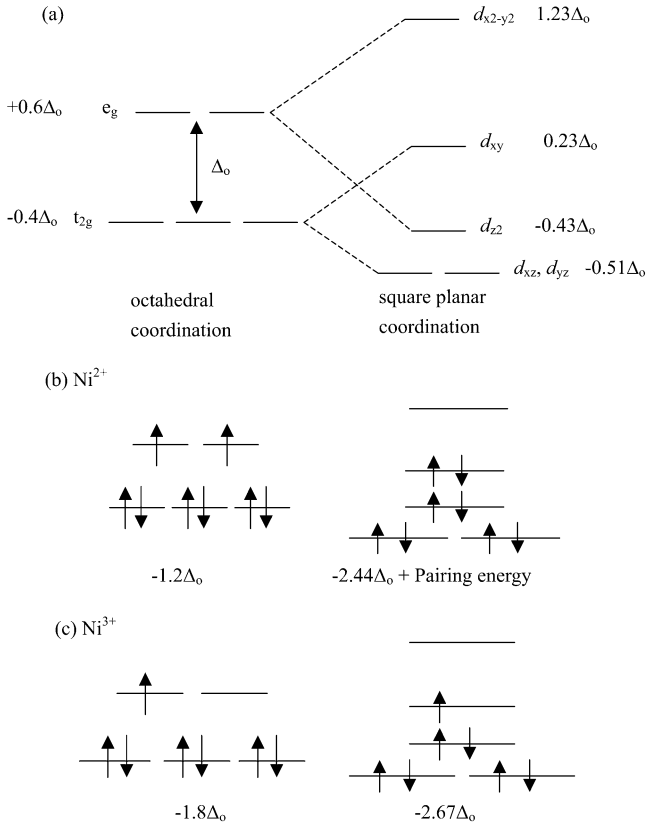

Figure 7. (a) *d*-Orbital splitting in square planar coordination (ref 14); (b) the case of Ni^{2+}; (c) the case of Ni^{3+}.

the orbitals split as shown in Figure 7a. Because of the reduction of overlap with the oxygen 2*p* orbital along the *z*-axis, the *d*-orbitals with a *z* component go down in energy. The d_{z2} orbital decreases relatively more than the d_{zx}, d_{yz} orbitals because its overlap with O_{2p} in an octahedron is larger. In contrast, the energies of the d_{x2-y2} and the d_{xy} orbitals increase because the oxygen ions in the $x-y$ plane typically move a little closer to Ni. The change in the levels has been taken from ref 13 and is based on an ion in an electrical field of point charge ligands.[14]

Assuming that the average *d*-level energy is constant in going from octahedral to square planar, the energies of Ni^{2+} (d^8) can be compared in these environments. While square planar clearly benefits from CFSE ($-2.44\Delta_o$ versus $-1.2\Delta_o$ for octahedral, where Δ_o is the octahedral crystal field splitting between the t_{2g} and e_g level), it comes with an exchange penalty in the d_{xy} level. In octahedral Ni^{2+} two unpaired electrons are in e_g levels, whereas Ni^{2+} in square planar has all doubly occupied levels, and no net spin. The pairing energy (i.e., the cost of having an electron with opposite spin in the same orbital) decreases the benefit of square planar over octahedral coordination. We estimated the electron pairing energy from DFT by comparing a magnetic calculation of 1T-Li_2NiO_2 with one where the magnetic moment was constrained to zero, thereby forcing both e_g electrons to occupy the same orbital, but with opposite spin. The resulting pairing energy is 0.79 eV. The octahedral gap Δ_o was estimated from the energy difference between the majority t_{2g} and e_g states in 1T-Li_2NiO_2 to be about 1.13 eV (Figure 8), in good agreement with literature values based on spectroscopic data.[15] The resulting CFSE of square planar Ni^{2+} over octahedral Ni^{2+} is 0.61 eV.

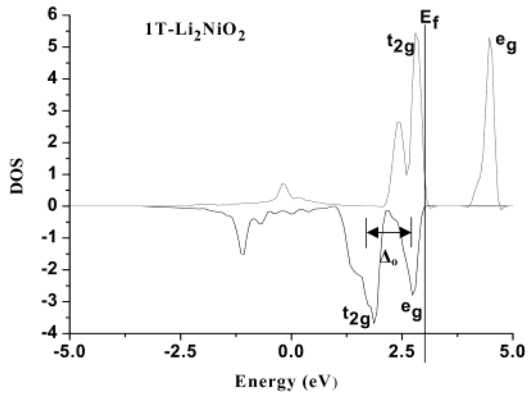

Figure 8. Density of states of 1T-Li_2NiO_2.

Rather than use the simple orbital diagram of Figure 7, we also estimated the CFSE directly from the calculated DOS by integrating the *d*-component of the DOS for each Ni^{2+} configuration up to the Fermi level. Before comparing the energies, the average energy of the *d*-states was adjusted to be same. The calculated result confirms the CFSE stabilization of square planar Ni^{2+} though by a slightly lower amount (0.48 eV).

The problem with the CFSE argument is that it would also stabilize Ni^{3+} in square planar environment, and by an even larger amount than for Ni^{2+}, as can be seen in Figure 7c. This is in clear contrast to the direct first principles result which indicates that the layered $LiNiO_2$ with octahedral Ni^{3+} is about 200 meV lower in energy than I-$LiNiO_2$. The discrepancy must come from the terms not accounted for in the CFSE such as the Li^+-Li^+ interaction and the long-ranged part of the Ni−O electrostatic interaction. Further evidence that it is not CFSE which stabilizes Ni^{2+} in a square planar comes from the fact that NiO forms a rocksalt structure with octahedral coordination, and not a structure with square planar environment.

The electrostatic interaction of Li is considerably different in both structures. Even though Li occupies the tetrahedral sites in both the 1T and *Immm* structure, the Li−Li distance in 1T-Li_2NiO_2 is about 10% less than that in I-Li_2NiO_2 according to the calculated bond lengths. Hence, the I-Li_2NiO_2 structure offers an electrostatically more favorable Li arrangement, and this is likely to be the dominant reason this structure is more stable than 1T-Li_2NiO_2. As shown previously, the spin pairing cost removes much of the CFSE gain for Ni^{2+} in a square planar environment making it unlikely to be stable over octahedral Ni^{2+} if no Li were present to further stabilize the structure.

Phase Transformation During Cycling. From the experimental results and the first principles calculations, it is shown that the *Immm* structure becomes unstable with delithiation. EXAFS, electrochemical observations, and first principles calculations all indicate that at some point the layered structure forms from the *Immm* structure during the cycling. However,

(14) Krishnamurthy, R.; Schaap, W. B. *Chem. Educ. J.* **1969**, *46*, 799.

(15) Cox, P. A. *Transition Metal Oxides*; Oxford University Press: New York, 1995; p 46.

Table 2. Energy Difference between the Layered Structure and *Immm* Structure with Doping

M	$Li_2Ni_{1-x}M_xO_2$ ($\Delta = E_{Immm} - E_{layered}$)	$LiNi_{1-x}M_xO_2$ ($\Delta = E_{Immm} - E_{layered}$)
Cu ($x = 0.25$)	−0.774	0.195
Pt ($x = 0.25$)	−1.176	0.295
Fe ($x = 0.25$)	−0.752	0.254
Cu ($x = 0.5$)	−0.779	0.214
nonsubstituted	−0.774	0.198

because of the different oxygen arrangement in these two structures, the long range ordering is expected to be lost during the transformation resulting in the observed pseudo-amorphous XRD pattern. Even though there may not be long range ordering, the electrochemical profile of the pseudo-amorphous material bears resemblance to that of the crystalline layered $LiNiO_2$. This illustrates the different characteristic length scales that determine the XRD and chemical potential of Li. While an XRD pattern is obtained from cumulative reflections over a relatively long ranged periodic array of atoms, the electrochemical intercalation reaction does not require periodicity over such a long range and is more affected by the local environment of Li. Therefore, we believe that after cycling the material has local fragments of the layered $LiNiO_2$ structure, but these fragments may only extend for a few lattice parameters. This picture is consistent with the EXAFS analysis which indicates that the short range ordering of Ni becomes more layerlike with delithiation as evidenced by the increase in the Ni−O coordination number. However, even in EXAFS the Ni−Ni coordination does not increase as much as the Ni−O coordination, indicating that there must be many very small clusters. Given that local ordering of Li and Ni in a layerlike structure occurs (as shown in the electrochemical result and EXAFS result), but the long range ordering is lost (as evidenced from the XRD), it can be concluded that nanosize structural domains of a layerlike structure form during cycling. It is also worthwhile to note that the coordination number of the Ni−Ni shell is 3.4 which is much less than 6, whereas that of Ni−O is 5.4

Chemical Substitution of Ni. Using first principles computations as a screening tool, we investigated various substitutions of Ni as a possible way of stabilizing the orthorhombic *Immm* structure during electrochemical cycling. Cu, Pt, and Fe, which have all been reported to occur in planar 4-fold coordination were substituted at the 25% and 50% levels.[16] The calculated results are shown in Table 2. For all the substituted materials, the orthorhombic *Immm* is more stable than the layered structure at $Li_2(Ni,M)O_2$ composition though Pt is the only element that increases the stability of the *Immm* structure over that of 1T-$Li_2(Ni,M)O_2$. However, as lithium is taken out from *Immm*, the stabilization of the *Immm* structure over the layered structure is decreased for all substitutions except Cu. Pt and Fe destabilize the I-$LiNiO_2$ relative to R$\bar{3}$m $LiNiO_2$, whereas Cu has a negligible effect.

Pt destabilizes the I-$LiNiO_2$ structure more than Fe or Cu because Pt^{2+} is difficult to oxidize compared with Fe^{2+} or Cu^{2+}. Therefore, when Pt is mixed with Ni in I-$LiNi_{0.75}Pt_{0.25}O_2$, it produces more Ni^{4+} which has been shown to be quite unstable as I-NiO_2. A suitable chemical substitution for Ni is not easy to find as it should both be stable in a 4-fold coordination that supports the orthorhombic *Immm* structure and minimize the production of Ni^{4+} by oxidizing itself to a higher oxidation state. Takeda et al. reported on the electrochemical properties of the Li_2CuO_2−Li_2NiO_2 solid solution.[17] In their electrochemical result, the first cycle profile was clearly different from the subsequent ones, and XRD patterns also showed a transformation into a pseudo-amorphous state after multiple cycles. These results agree with our prediction that even with Cu doping, the *Immm* structure is not stable against delithiation.

Conclusion

Li_2NiO_2 in the *Immm* structure was synthesized by a solid-state reaction, and its electrochemical behavior upon delithiation was evaluated. From the electrochemical data, first principles calculation, and EXAFS analysis, it is suggested that the *Immm* structure transforms to the layered structure during the first cycle. First principles computations of some chemically substituted materials identified Pt substitution as a way of stabilizing the $Li_2(Ni,M)O_2$ composition in the *Immm* structure but found no elements that would likely stabilize the material upon Li removal.

Acknowledgment. We thank Prof. Yang Shao Horn for the valuable discussion. This work was supported by the MRSEC Program of the National Science Foundation under award DMR 02-13282, by the Assistant Secretary for Energy Efficiency and Renewable Energy, Office of FreedomCAR and Vehicle Technologies of the U.S. Department of Energy under Contract DE-AC03-76SF00098, Subcontract 6517748 with the Lawrence Berkeley National Laboratory, and in part by the Ministry of Education of Taiwan (EX-91-E-FA09-5-4). We are grateful to Dr. Dane Morgan, Fei Zhou, Dr. Anton Van der Ven, Dr. Dany Carlier, Chris Fischer, and Tim Mueller for their advice.

CM049922H

(16) Shannon, R. D. *Acta Crystallogr. A* **1976**, *32*, 751.

(17) Imanishi, N.; Nishijima, M.; Hirano, A.; Ikenishi, T.; Takeda, Y. Presented at Lithium Battery Discussion, Electrode Materials, Bordeaux-Arcachon, France, September 14−19, 2003, Abstract No. 99.